Coreless, Contactless Power Supply System with DSP Controlled Active Compensation of Parameter Changes

M. Marcinek[1], M. Holub[1]
[1]*West Pomeranian University Of Technology, Department of Electrical Engineering*
ul. Sikorskiego 37, 70–313 Szczecin, Poland
marcin.holub@zut.edu.pl

[1]***Abstract*—Contactless power supply systems are of high interest in small power and large power applications. Many high efficiency contactless systems use the resonant operation mode. A parallel compensation system is presented enlarging overall system safety and allowing for resonant system parameter change while maintaining zero current switching (ZCS) operation. Basics of digital control unit construction and operation are presented. Simulation and experimental results are given for control system operation. Systems performance allows for large resonant circuit parameter drift. Modern DSP control unit minimizes the necessary external circuitry and time delays in case of most important operations.**

***Index Terms*—Contactless Power Supply, digital control systems, high frequency power converter, wireless power transmission, ZCS converters.**

I. INTRODUCTION

Contactless power supply is a rapidly developing technology field, most of all in recent years. Some commercial products are already available as mobile computer charging stations or contactless charging stations for customers' electronic devices. Some contactless solutions use a coreless transformer which construction is based on PCB winding layout without a ferrite core [1], [2]. Applications covering larger powers are of highest interest because of the increase of overall convenience and safety and because of possible implementations in automotive and transportation industries [3]–[5]. These systems can be used for instance as a battery chargers [6], [7], that can deliver power during idle time of the vehicle. Advantages of coreless systems are that they have smaller weight and increased mechanical durability because of the absence of the ferrite core. Moreover the shape design of primary and secondary coils is more flexible.

Currently many actions are under scientific investigation covering a wide span of studies. For instance the shape and type of magnetic circuit [8], relationship between the size and shape of the primary and secondary circuits [9], [10] and power electronic units [11], [12] are under investigation.

This work concentrates on a typical series-resonance contactless power supply circuit with a parallel resonance compensator. Proposed compensator is connected in parallel to system's resonant capacitor. Another possibility includes the use of an additional capacitor as described in [13], [14].

Manuscript received December 14, 2013; accepted August 2, 2014.

Proposed solution is shown in Fig. 1 and is based on a well-known series resonance circuit with a full bridge excitation system, a solution often used in energy transfer systems [1], [8], [15], [16]. In many cases the primary side of the high frequency transformer (often coreless) is used as system's resonant inductance. The secondary side usually supplies the load using many individual solutions including resonant secondary circuits or a typical rectifier circuit.

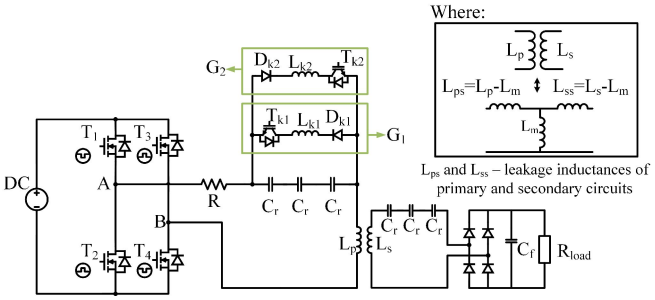

Fig. 1. Proposed contactless power supply topology with an active compensation circuit.

$$f_r = f_0\sqrt{1-\frac{1}{4Q^2}}, \tag{1}$$

where

$$Q = \frac{1}{R}\sqrt{\frac{L}{C}}, \tag{2}$$

and

$$f_0 = \frac{1}{2®\sqrt{LC}}. \tag{3}$$

II. BASICS OF OPERATION

Proposed contactless power converter topology is shown schematically in Fig. 1. It includes a main, full bridge power converter and the additional, parallel compensation unit compromising two parallel branches: the first one (G_1) including the power transistor T_{k1}, diode D_{k1} and the inductor L_{k1}, and the second one (G_2) including the power transistor T_{k2}, diode D_{k2} and the compensating inductor L_{k2}.

At the secondary side of a coreless transformer the load unit is

introduced consisting of a rectifier, smoothing capacitor C_f and the load represented by a resistor R_{load}. Such topology allows a constant current conduction in the compensator unit which in consequence allows to increase the span of resonant frequencies of system operation with regard to the solution presented in [17].

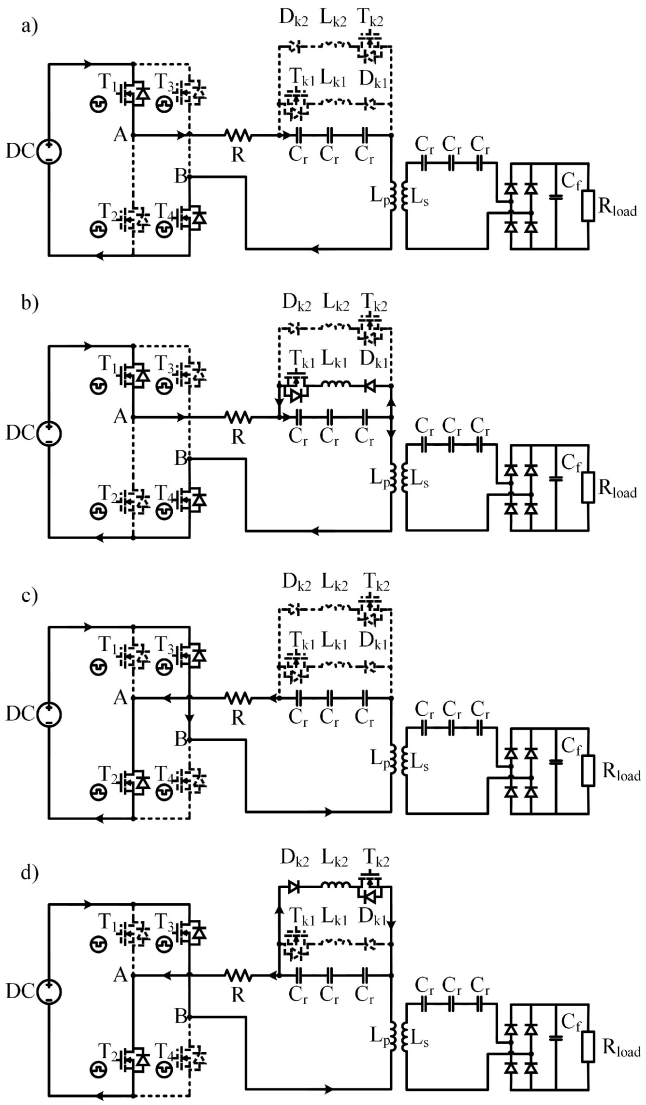

Fig. 2. Basics of operation of the power supply with the compensator unit.

Inductance L_{ps} (from Fig. 1) together with three serially connected capacitors C_r constitute the resonant circuit. Purpose of the series connection of capacitors was that in laboratory test-stand high values of voltage across the resonant circuit can develop. That solution allows to reduce relative voltage at each capacitor.

In this simple case the switching frequency f_f of power transistors should be set equal to the resonance frequency f_r described with a very well-known equation [15]. Resulting from (2) and (3) the secondary versus primary side position and distance (influencing the value L) or load variation (influencing the value R) will change the resonant frequency f_r. In such case the proposed compensator operation should return system's resonant frequency to the initial value of f_r. Similarly to a reactive power compensator using the control delay angle „α" overall system reactance can be adjusted.

In order to control the compensation unit a synchronization with the main, full bridge circuit is required. In presented solution the resonant voltage zero crossing point of the voltage across the C_r capacitor is used.

In order to explain basics of operation of the circuit energy flow paths (Fig. 2) and corresponding time waveforms (Fig. 3) will be discussed. Presented time domain waveforms are shown only for primary side of the system, operation of the secondary side is not considered in this paper. In Fig. 2 arrows and solid lines represent the current flow direction and active parts of the topology respectively.

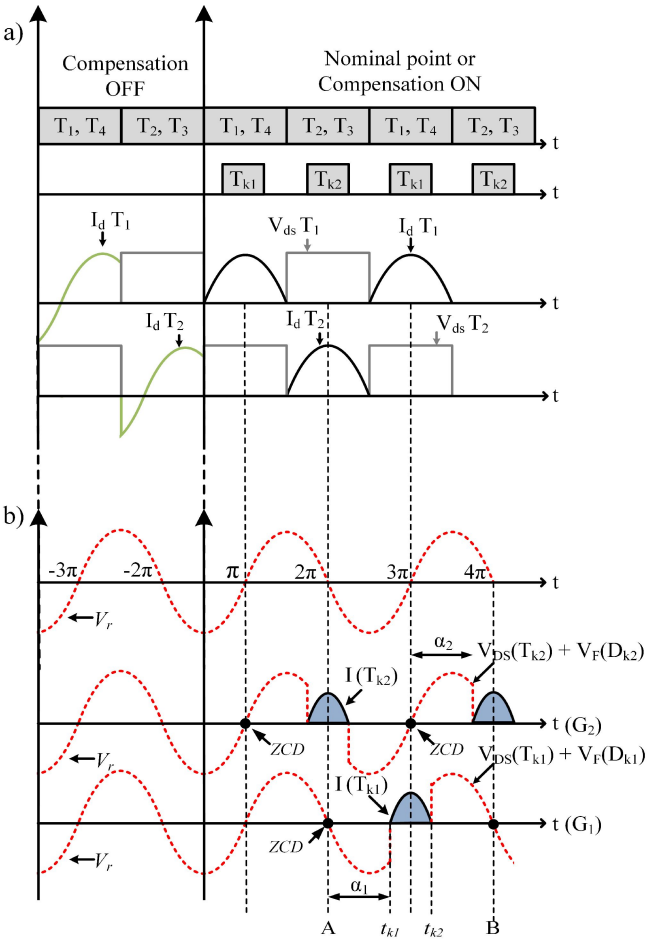

Fig. 3. Basic time domain waveforms.

Initially (Fig. 2(a)) the main circuit transistors T_1 and T_4 are switched on allowing for resonant circuit $(3 \times C_r) - L_{ps}$ recharge. After the recharge half-period the conducting transistors should be changed and T_2 together with T_3 should begin conduction (Fig. 2(c)). In case of constant parameter values the resonant circuit current and voltage are sinusoidal and no compensation is necessary, system operates in the resonance point (ZCS) using only states of operation given in Fig. 2(a) and Fig. 2(c). Corresponding waveforms, for this state was presented in Fig. 3(a), in section called "Nominal Point".

In Fig. 3(a), in the part named "Compensation OFF" a state when system parameter or load change was presented and as result f_r decrease it's value. After the resonant frequency change and if main power transistors are still operated with a constant frequency f_f (which value is equal to frequency of natural resonant point) no ZCS operation is possible and system losses increase as presented in Fig. 4. Simulations were led using a detailed IGBT loss model in PLECS simulation environment. Losses in the natural resonance point are referred to as $P_{loss\ nom}$.

Voltage across the one C_r capacitor is referred to as V_r. The control signal of power transistor which is part of branch G_2

should be synchronized with the voltage V_r. For this branch synchronization point is obtained when resonance voltage changing its value from negative to positive, while the G_1 branch should be synchronized with the change from positive to negative. Regarding angular frequency domain their shift against each other is set at the value of π. Synchronization means that this is starting point when delay angle is counted. After that control unit will puts proper transistor in to conduction.

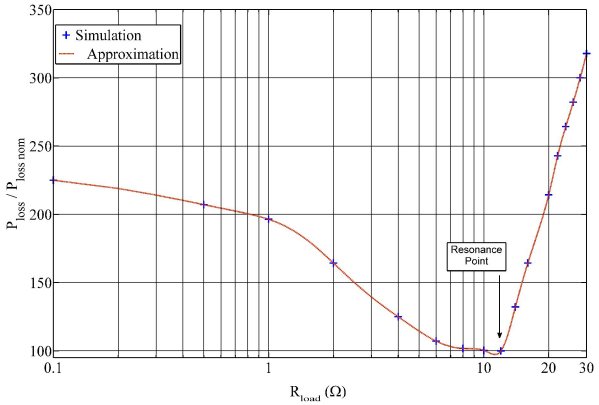

Fig. 4. Relative semiconductor losses for different load conditions; no compensation.

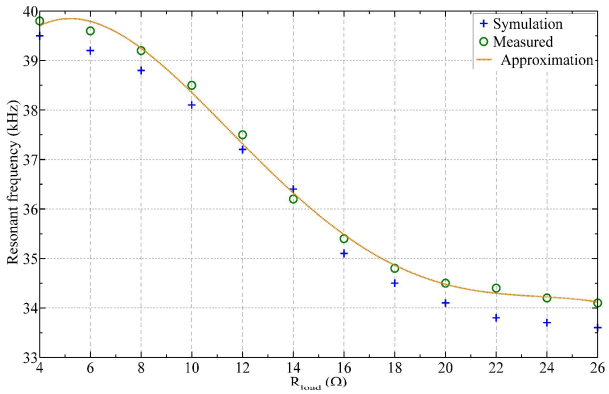

Fig. 5. Resonant frequency change as a function of load resistance.

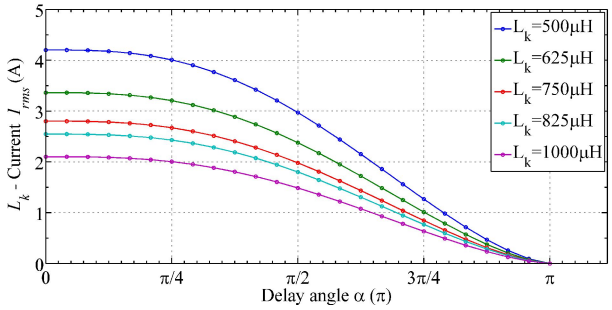

Fig. 6. Compensator I_{rms} current value as a function of delay angle α and compensator inductance L_k.

As mentioned above the voltage V_r is monitored and from the zero crossing point the delay time is calculated in order to control the amount of energy delivered to the compensator unit.

In case of zero crossing from positive to negative values the time delay α_1 is defined between time points A ÷ t_{k1} in Fig. 3(b). After that time delay compensator transistor T_{k1} is switched on allowing for C_r – T_{k1} – D_{k1} – L_{ps} circuit current flow (Fig. 2(b)). Symmetrically if the V_r changes from negative to positive an identical amount of time delay, defined as α_2, is used in order to control the control signal of the T_{k2} transistor (Fig. 2(d)). The time at which selected branch was conducting is indicated by t_{k1} – t_{k2} and it is related with the angle α. In that case relative value of I_{rms} will change. It can be expressed as follows

$$I_{rms} = \frac{U}{\mu L}\sqrt{\frac{1}{4®}\left(2® - 2\sim - \frac{1}{2}(\sin(4® - 2\sim) - \sin(2\sim))\right)}. \quad (4)$$

Equation (4) assumes purely inductive character of the compensator circuit. In Fig. 6 calculated values of I_{rms} current were presented.

It is worth to notice that no negative current is possible in the compensator branches due to the use of blocking diodes, all transistors in the system are switched using the zero current switching technology (Fig. 3). Such compensator unit construction and operation allows for system parameter and/or load change during resonant operation with constant frequency of operation of the main circuit transistors. A more detailed analysis of circuit operation can be found in [18].

Figure 5 presents graphically the dependency between circuit resonance frequency f_r and system load. Variable load was modelled using variable load resistance. As can be noticed, in order to maintain ZCS with no compensation the main supply bridge should change its frequency of operation with relation to presented function. It is not possible in this case to operate under constant frequency.

In such case proposed compensator should be operated with a properly chosen delay angle α. The delay angle can be set in the range of 0° ÷ 180° electric allowing for natural resonance frequency change in the range of 10 kHz (for compensator inductances of 750 μH).

III. RESONANT CIRCUIT DIGITAL CONTROL UNIT

Figure 7 depicts the conceptual drawing of control system construction. As a source of information of the control circuitry V_r, drain – source voltage V_{ds} and transistor currents I_r are measured. Based on measured signals the control unit synchronizes all transistor gates and in addition has an influence on the V_{dc} – the supply voltage level. Wireless Bluetooth communication modules are used in order to visualize and record parameter values on a remote PC computer.

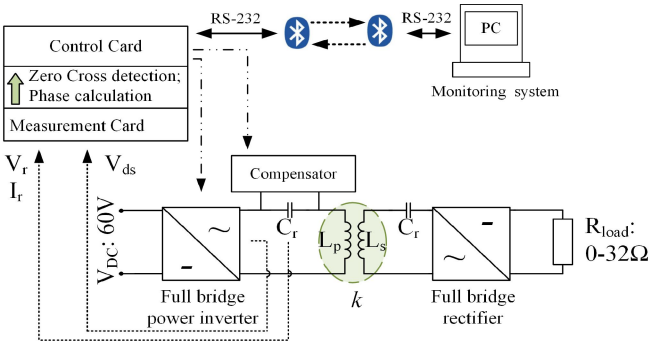

Fig. 7. Basic configuration of proposed contactless series resonance power supply with parallel compensator and a digital control unit.

A digital signal processor DSP F28335 from Texas Instruments C2000 family was used. The choice was met in accordance with main processor properties as a number and functionality of peripheries, six hardware supported PWM modules. In addition this controller family supports the use of enhanced capture module mode allowing for fast (6,6 e-9s) and accurate (32 bit) phase angle measurement between V_{ds} and the transistor drain current I_d.

The main reason of F28335 controller platform utilization was the frequency of CPU unit operation. It is triggered with 150 MHz which results in 6.66e-9s cycle time.

This will in the future allow to find new delay angle α value automatically using only a limited number of PWM periods. All peripheries of proposed controller platform are supplied with 3.3 V, due to that fact and because of necessary separation of power electronic circuits and the controller board an interface board was proposed. Main tasks of additional circuitry include a conversion of analog signals into appropriate digital markers, fast analog to digital 12 bit conversion of main circuit currents and voltages in order to protect the power switches and voltage amplitude conversion. A general structure of proposed interface card is presented in Fig. 8.

A. Current, Voltage and Phase Angle Digital Markers

In order to control the compensator circuit a phase angle between transistor current and voltage needs to be identified. Measurement of both quantities is done using voltage and current transducers.

Bridge output current is measured using TALEMA AS-102 transducer. In further processing a digital current marker is introduced displaying the timeframe in which the current half-period flows through a defined bridge diagonal. Two voltage measurements are also proposed including the resonant capacitor C_r voltage V_r and the drain – source voltage of the T_2 power transistor. Resonant capacitor voltage V_r is measured using a transformer, due to high frequency and voltage a transfer ratio n_2/n_1 equal to 14/2000 is proposed. Transistor drain-source voltage V_{ds} was measured using a passive voltage divider. Using fast voltage comparators LM7219 and AD790 measured signals are compared with references (Fig. 8) and their digital markers are constituted. A logical EXOR combination of output current I_{t2} and transistor voltage V_{ds} markers contribute to phase angle digital marker construction. Two examples of such approach are presented in Fig. 9(a) and Fig. 9 Fig. 9(b). A practical verification of such approach is depicted in Fig. 10. Signal I_{t4} is obtained from I_r using AND gate and V_{ds} signal on the second input.

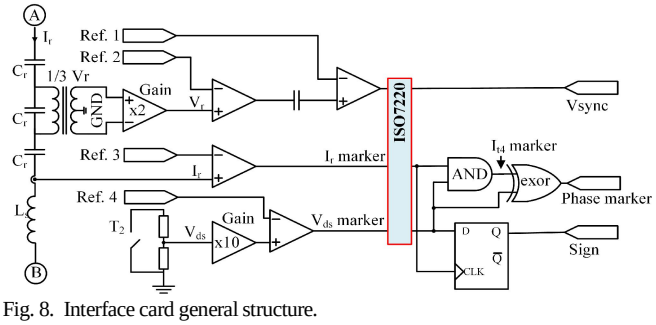

Fig. 8. Interface card general structure.

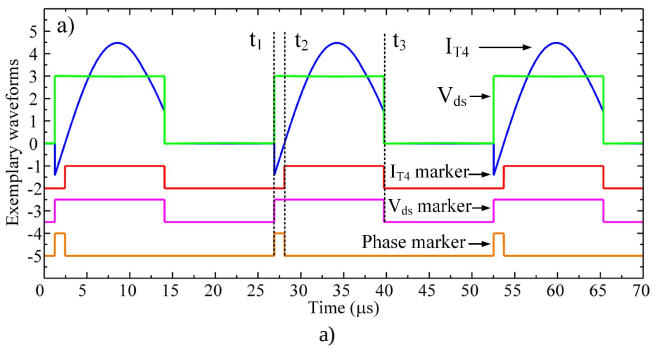

a)

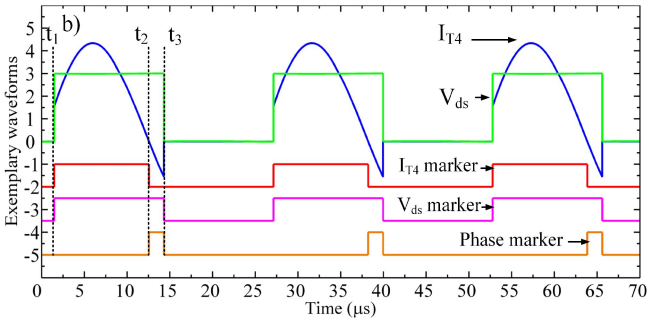

b)

Fig. 9. Exemplary waveforms for digital voltage, current and phase angle markers for: a) $f_f > f_r$; b) $f_f < f_r$.

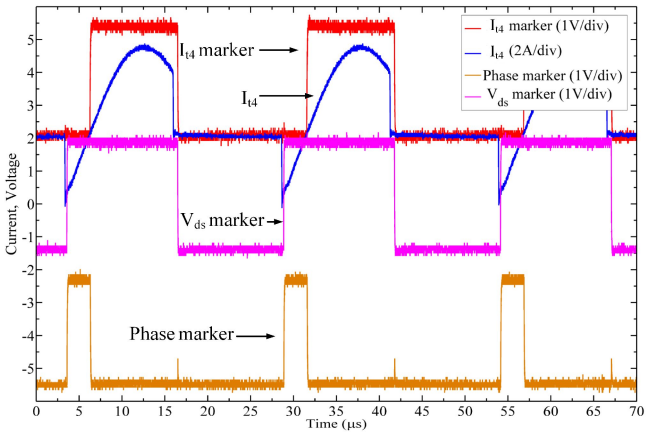

Fig. 10. Practical verification of phase angle marker construction for unsynchronized system operation.

B. Phase Angle Marker Sign

In order to verify if system operation is below or over the natural resonant frequency (Fig. 9(a), Fig. 9(b)) and additional phase angle marker sign is introduced. A D-type flip-flop was used for this purpose. Data input is assigned to V_{ds} signal digital marker, I_r signal digital marker was assigned to clock input of the flip-flop. In case V_{ds} is equal to logical one when I_r marker appears, V_{ds} is beforehand I_r in phase and the flip-flop will produce a digital one on its output. This should lead to a stronger compensator influence and therefore α angle minimization. In opposite case the flip-flop will produce a logical zero suggesting for compensation circuit influence minimization and therefore α angle increase.

C. Resonance Voltage Zero Cross Point Detection

Resonance voltage V_r is measured, as previously mentioned, using a measurement transformer. Based on this measurement a zero crossing point detection V_{sync} mechanism is proposed implementing two fast voltage comparators (Fig. 8).

The first comparator AD790 is implemented in order to detect the zero crossing point. The output of the first comparator, through a derivative capacitor, is introduced to non-inverting input of a LT1720 comparator. This pulses are compared to externally set reference voltage. Such a mechanism is proposed in order to minimize the influence of external noise and false zero-crossing point detection. Applied DSP platform includes an input qualification mechanism allowing to reject pulses that are shorter than a defined duration.

Zero crossing point signal V_{sync} is used in order to control the main bridge in resonant mode. It triggers the interrupt flag that synchronizes PWM modules of the DSP. Used processor

platform requires only 220 ns delay time between the zero cross point detection and PWM synchronization.

IV. SIMULATION AND EXPERIMENTAL RESULTS

A. Simulations

As mentioned before PLECS 3.3 was used for model based simulations. Performed calculations allowed to examine the influence of different geometrical configurations of the primary and secondary side of coreless power supply as well as the sensitivity to load variations (Fig. 5). In addition the range of possible parameter changes that can be compensated was obtained and influence of parameter changes on transistor losses in non-compensated circuit was examined (Fig. 4). Parameters used for calculations and their comparison to measured parameters of the prototype are summarized in Table I.

TABLE I. CIRCUIT PARAMETERS USED IN SIMULATION MODEL AND MEASURED VALUE OF THE PARAMETER OF THE CONSTRUCTED PROTOTYPE.

Name	Simulation Component Value	Prototype Component Value	
C_r [nF]	110	112	
R_{load} [Ω]	0 - 32		
L_p [μH]	208	207	
L_s [μH]	208	208	
L_{k1} and L_{k2} [μH]	750	737	768
k factor	0,3	0,29	

Figure 11 summarizes simulation results of compensator delay angle sensitivity to parameter variations. Load resistance change and primary – secondary (transmitter – pickup) side position shifts were studied. As a result of position alternations magnetic coupling factor k was adjusted.

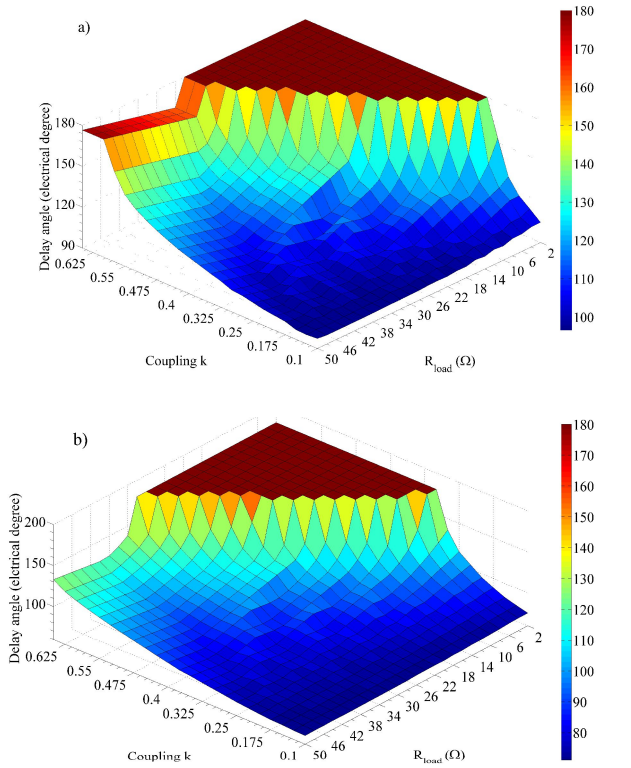

Fig. 11. Delay angle sensitivity for different loads and transformer couplings for natural resonant frequency: a) f_f = 37 kHz, b) f_f = 39 kHz.

As can be noticed a delay angle surface can be obtained for different initial parameters resulting in variable initial natural frequency f_r. A large parameter drift can be compensated in parallel to varying load conditions. No instabilities were found which simplifies future closed loop control system.

B. Prototype Construction and Experimental Results

In order to verify practical properties of proposed power supply construction, compensator influence and digital control system properties a 350 W prototype was designed and constructed. Photographs of prototype construction are presented in Fig. 12. Test stand includes a full bridge power electronic converter (1), proposed parallel compensator unit (2), DSP based control system and interface cards (3), auxiliary DC power supply units for electronics (4). The bottom part presents constructed coreless transformer circuit consisting of the secondary (5) pick-up side and primary (6) transmitter side. All oscilloscope waveforms were obtained using a Tektronix DPO 4054.

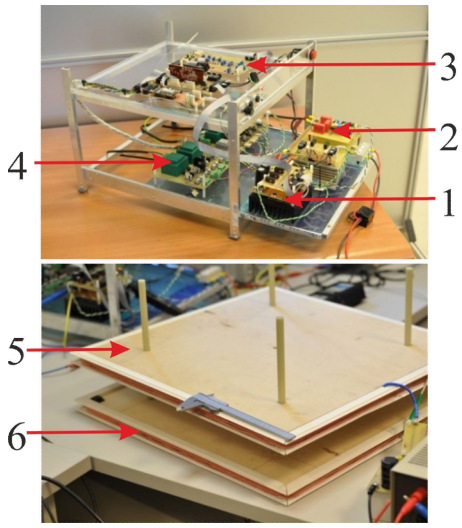

Fig. 12. Prototype construction: top) power electronic converter with compensator circuit and a digital control system, bottom) coreless primary and secondary side of the prototype.

An exhaustive set of experiments was led in order to examine properties obtained using simulation modelling. Load variation sensitivity was examined, results comparison is presented in Fig. 5 (green circles). As can be noticed good agreement with simulation results was achieved, a nonlinear system characteristics of load variation was experimentally validated.

Compensator control functions were investigated. For three different coreless, contactless supply unit distances and identical load resistance value of 20 Ω necessary compensator unit phase angle delay α was found allowing for ZCS operation. A comparison of simulation and experimental results is presented in Table II.

TABLE II. CALCULATED AND MEASURED COMPENSATOR DELAY TIMES FOR DIFFERENT PRIMARY – SECONDARY SIDE DISTANCES.

	f_r (kHz)	R_{load} (Ω)	Delay angle α simulated degree electric	Delay angle α measured degree electric
a)	39,5	20	92,8°	91,68°
b)	37,2	20	119,5°	121,9°
c)	34,1	20	---	---

Typical measurement results are depicted in Fig. 13(a), Fig. 13(b). Delay angle α is graphically presented for two different pickup coil positions. As can be noticed ZCS action of power transistors is validated. Necessary compensator delay

angle α was measured for setups as in Table II (a), (b). For 34,1 kHz natural resonance frequency occurred and in consequence no compensator action was required.

Obtained simulation and experimental waveforms are in very good agreement. This leads to the conclusion that the used simulation model is adequate. Performed analyses allow for future closed loop control system with automatic compensator adjustment and delay angle controller.

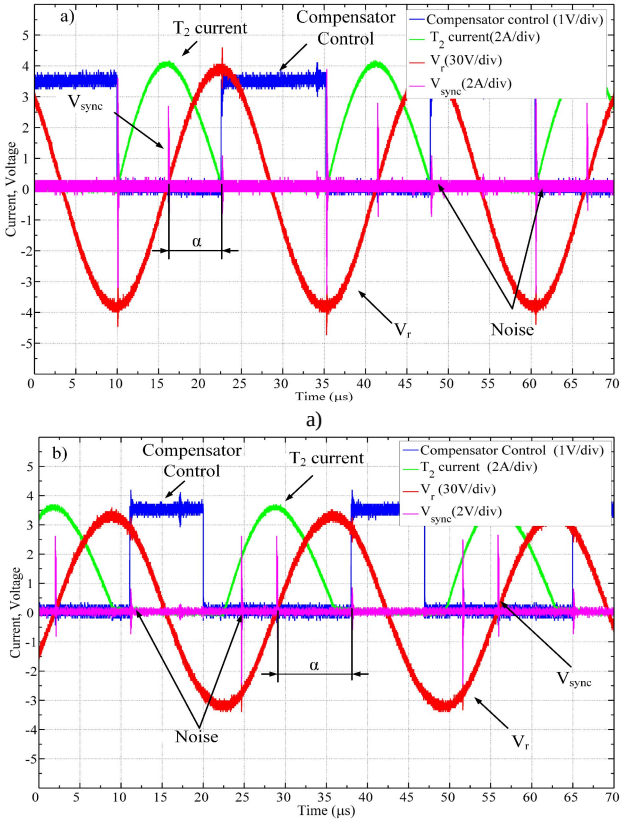

Fig. 13. Basic main bridge and compensator waveforms for two different pickup coil distances: a) f_r = 39,5 kHz – larger compensating action, b) f_r = 37,2 kHz – smaller compensating action.

V. CONCLUSIONS

A unique contactless, coreless power supply system was presented operating in the series resonance mode. An active, parallel compensation circuit is proposed allowing large parameter change and load variation. For proposed topology the natural resonance frequency of the system can change in the range of 10 kHz with 750 μH compensator inductance.

A digital, DSP based control system is proposed with analog circuitry performing current and voltage conversion into digital markers. A phase – shift sign recognition mechanism is proposed allowing for future closed loop control of the compensating unit. Wireless transmission of power supply data into remote PC computer was implemented.

Simulation model was constructed and simulation results are presented. Sensitivity to load changes was examined as well as switching loss increase of power transistors in case of no-compensated circuit operation. Compensator control circuit properties were investigated and necessary delay angles for different transmitter – pickup coil positions were found.

Practical verification of simulated waveforms and properties was performed using a 350 W prototype. Very good agreement of experimental data with simulated values was obtained. Future work will include an automatic tuning system with closed loop compensator operation.

REFERENCES

[1] P. Meyer, P. Germano, M. Markovic, Y. Perriard, "Design of a contactless energy-transfer system for desktop peripherals", *IEEE Trans. Industry Applications*, vol. 47, pp. 1643–1651, 2011. [Online] Available: http://dx.doi.org/10.1109/TIA.2011.2153812

[2] S. Y. R. Hui, W. W. C. Ho, "A new generation of universal contactless battery charging platform for portable consumer electronic equipment", *IEEE Trans. Power Electronics*, vol. 20, no. 3, pp. 620–627, 2005. [Online] Available: http://dx.doi.org/10.1109/TPEL.2005.846550

[3] M. Ibrahim, L. Pichon, L. Bernard, A. Razek, J. Houivet, O. Cayol, "Advanced modeling of a 2kW series-series resonating inductive charger for real electric vehicle", *IEEE Trans. on Vehicular Technology*, vol. 99, pp. 1–1, 2014. [Online] Available: http://dx.doi.org/10.1109/TVT.2014.2325614

[4] Rui Chen, Cong Zheng, Z. U. Zahid, E. Faraci, Wengsong Yu, Jih-Sheng Lai, M. Senesky, D. Anderson, G. Lisi, "Analysis and parameters optimization of a contactless IPT system for EV charger", *Twenty-Ninth Annual IEEE Applied Power Electronics Conf. and Exposition (APEC)*, 2014, pp. 1654–1661. [Online] Available: http://dx.doi.org/10.1109/APEC.2014.6803528

[5] O. C. Onar, M. Chinthavali, S. Campbell, Puqi Ning, C. P. White, J. M. Miller, "A SiC MOSFET based inverter for wireless power transfer applications", *Twenty-Ninth Annual IEEE Applied Power Electronics Conf. and Exposition (APEC)*, 2014, pp. 1690–1696. [Online] Available: http://dx.doi.org/10.1109/APEC.2014.6803533

[6] I. Jabri, F. Ghodbane, A. Bouallegue, A. Khedher, "Analysis of the coreless transformer in wireless battery vehicle charger", *Ninth Int. Conf. on Ecological Vehicles and Renewable Energies (EVER)*, 2014, pp. 1–6. [Online] Available: http://dx.doi.org/10.1109/EVER.2014.6844054

[7] J. Sallan, J. L. Villa, A. Llombart, J. F. Sanz, "Optimal design of ICPT systems applied to electric vehicle battery charge", *IEEE Trans. Industrial Electronics*, vol. 56, no. 6, pp. 2140–2149, 2009. [Online] Available: http://dx.doi.org/10.1109/TIE.2009.2015359

[8] Y. Nagatsuka, N. Ehara, Y. Kaneko, S. Abe, T. Yasuda, "Compact contactless power transfer system for electric vehicles", *in Proc. Power Electronics Conf. (IPEC)*, Sapporo, 2010, pp. 807–813. [Online] Available: http://dx.doi.org/10.1109/IPEC.2010.5543313

[9] E. Waffenschmidt, T. Staring, "Limitation of inductive power transfer for consumer applications", *in Proc. of EPE Conf.*, Barcelona, 2009.

[10] Trong-Duy Nguyen, Siqi Li, Weihan Li, C. C. Mi, "Feasibility study on bipolar pads for efficient wireless power chargers", *Twenty-Ninth Annual IEEE Applied Power Electronics Conf. and Exposition (APEC)*, 2014, pp. 1676–1682. [Online] Available: http://dx.doi.org/10.1109/APEC.2014.6803531

[11] F. Pijl, P. Bauer, M. Castilla, "Control method for wireless inductive energy transfer systems with relatively large air gap", *IEEE Trans. Industrial Electronics*, vol. 60, pp. 382–390, 2013. [Online] Available: http://dx.doi.org/10.1109/TIE.2011.2163917

[12] L. J. Chen, G. R. Nagendra, J. T. Boys, G. A. Covic, "Double-coupled systems for roadway IPT systems", *Twenty-Ninth Annual IEEE Applied Power Electronics Conf. and Exposition (APEC)*, 2014, pp. 1618–1625. [Online] Available: http://dx.doi.org/10.1109/APEC.2014.6803523

[13] Ping Si, Aiguo Patrick Hu, D. Budgett, S. Malpas, J. Yang, Jinfeng Gao, "Stabilizing the operating frequency of a resonant converter for wireless power transfer to implantable biomedical sensors", *in Proc. 1st Int. Conf. Sensing Technology*, Palmerston North, 2005.

[14] Ping Si, Aiguo Patrick Hu, S. Malpas, D. Budgett, "A frequency control method for regulating wireless power to implantable devices", *IEEE Trans. Biomedical Circuits and Systems*, vol. 2, pp. 22–29, 2008. [Online] Available: http://dx.doi.org/10.1109/TBCAS.2008.918284

[15] Aigu Patrick Hu, *Wireless/Contactless Power Supply: - Inductively Coupled Resonant Converter Solutions*. VDM-Verlag, 2009.

[16] U. K. Madawala, M. Neath, D. J. Thrimawithana, "A power–frequency controller for bidirectional inductive power transfer systems", *IEEE Trans. Industrial Electronics*, vol. 60, pp. 310–317, 2013. [Online] Available: http://dx.doi.org/10.1109/TIE.2011.2174537

[17] J. James, J. Boys, G. Covic, "A variable inductor based tuning method for ICPT pickups", in *Proc. 7th Power Engineering Conf., IPEC*, Singapore, 2005, pp. 1142–1146. [Online] Available: http://dx.doi.org/10.1109/IPEC.2005.207079

[18] S. Kalisiak, M. Marcinek, M. Holub, R. Palka, "Contactless power supply system with resonant circuit parameter change compensation", in *Proc. Power Electronics and Applications (EPE 2011)*, Birmingham, 2011.